ELSEVIER

Solid State Ionics 154–155 (2002) 735–739

SOLID STATE IONICS

www.elsevier.com/locate/ssi

Electronic structures of protonic conductors $SrTiO_3$ and $SrCeO_3$ by O 1*s* X-ray absorption spectroscopy

T. Higuchi [a,*], T. Tsukamoto [a], N. Sata [b], M. Ishigame [b], K. Kobayashi [c], S. Yamaguchi [d], S. Shin [e,f]

[a] *Department of Applied Physics, Tokyo University of Science, 1-3 Kagurazaka, Shinjuku, Tokyo 162-8601, Japan*
[b] *Research Institute for Scientific Measurements, Tohoku University, Sendai 980-8577, Japan*
[c] *National Institute of Materials and Engineering, Tsukuba 305-8565, Japan*
[d] *Nagoya Institute of Technology, Nagoya 466-8555, Japan*
[e] *Institute for Solid State Physics, University of Tokyo, Chiba 277-8581, Japan*
[f] *RIKEN, Hyogo 679-5143, Japan*

Accepted 19 March 2002

Abstract

The electronic structures of protonic conductors $SrTi_{1-x}Sc_xO_3$ and $SrCe_{1-x}Yb_xO_3$ have been studied by O 1*s* X-ray absorption spectroscopy (XAS). In $SrTi_{1-x}Sc_xO_3$, hole state and acceptor-induced level are observed in the band gap energy region. Such a structure is also observed in the O 1*s* XAS spectra of $SrCe_{1-x}Yb_xO_3$. The XAS structures and their temperature dependence reflect the activation energy estimated from electrical conductivity. These facts indicate that the conductivity is achieved by deep acceptor-induced level lying in the middle of the band gap.

Keywords: Proton; Hole; Acceptor; $SrTi_{1-x}Sc_xO_3$; $SrCe_{1-x}Yb_xO_3$; XAS; Electronic structure

1. Introduction

It is well known that some perovskite-type oxides, such as $CaZrO_3$, $SrTiO_3$ and $SrCeO_3$, exhibit remarkable proton conductivity when they are doped with a few mol% of acceptor ions [1–5]. Oxide-type protonic conductors are very important materials for a wide variety of electrochemical applications such as fuel cells or hydrogen sensors because of their promise protonic conductivity at high temperature. Since proton-conducting perovskite oxides were discovered by Iwahara et al. [1], various investigations have been made to clarify its origin and nature. However, only little information is available at present on the transport properties and electronic structure [6–8].

Recently, the electronic structures of proton-conducting perovskite oxides $CaZrO_3$ and $SrTiO_3$ have been studied by photoemission spectroscopy (PES) and X-ray absorption spectroscopy (XAS) [9–13]. In the PES spectra of In-doped $CaZrO_3$, the Fermi level (E_F) shifts to the conduction band side by about 1.0 eV through proton doping [11]. Furthermore, in the O 1*s* XAS spectrum of In-doped $CaZrO_3$ is found the existence of holes at the top of the valence band [12]. The intensity of spectral features due to holes decreases with proton doping. Such a behavior is also

* Corresponding author. Tel.: +81-3-5228-8241; fax: +81-3-3260-4772.
E-mail address: higuchi@rs.kagu.tus.ac.jp (T. Higuchi).

0167-2738/02/$ - see front matter © 2002 Elsevier Science B.V. All rights reserved.
PII: S0167-2738(02)00474-5

found in the O 1*s* XAS spectra of Sc-doped $SrTiO_3$ [13]. These facts are consistent with the change of the amounts of hole, oxygen vacancy, and proton estimated by the defect chemical analysis, indicating that doped proton exchanges with holes.

In this study, the electronic structure of protonic conductor Sc-doped $SrTiO_3$ has been investigated by careful measurements using high resolution and high brightness O 1*s* XAS. XAS is related directly to the unoccupied state. The XAS gives the spectrum relating to the site- and symmetry-selected DOS. Therefore, high-resolution XAS is a powerful tool for the study of electronic structure in the band gap energy region and to relate it to the transport properties [14]. As references, the O 1*s* XAS spectra of undoped $SrCeO_3$ and Yb-doped $SrCeO_3$ ($SrCe_{0.95}Yb_{0.05}O_3$) were also measured.

2. Experimental

The sample was prepared by the solid state reaction of $SrTiO_3$, $SrCO_3$, and Sc_2O_3 at 1200 °C for about 12 h, and the single crystals were grown by a floating zone method using Xe-arc imaging furnace. The single crystals were grown in an atmosphere of oxygen to prevent protons entering the crystal. The Sc^{3+} ion is clear to be doped as an acceptor ion in the Ti^{4+} ion site of $SrTiO_3$ by a simple thermoelectromotive power experiments. The electrical conductivity measurements were performed by using an LCR meter (HP4275A) [4]. The sintered pellet of Yb-doped $SrCeO_3$ was prepared by the solid state reaction of $SrCO_3$, CeO_2, and Yb_2O_3 at 1400 °C for about 16 h. The samples of $SrCe_{1-x}Yb_xO_3$ and $SrTi_{1-x}Sc_xO_3$ were confirmed as being a single phase with perovskite structure by the powder X-ray diffraction analysis.

XAS measurements were carried out at the revolver undulator beamline BL-19B at the Photon Factory (PF) of the High Energy Accelerator Organization (KEK), Tsukuba in Japan. Synchrotron radiation from the undulator was monochromatized using a grating monochromator. The XAS spectra were measured by collecting the total fluorescence yield. The resolution of about $\Delta E/E = 5000$ at $h\nu = 400$ eV and high photon flux of about 10^{12}–10^{13} photons/s is realized with the spot size of 100 μm [15].

3. Results and discussions

Fig. 1 shows the O 1*s* XAS spectra as a function of Sc doping in $SrTi_{1-x}Sc_xO_3$ ($x = 0$–0.10). It has been already clarified that the O 1*s* XAS spectra of $SrTiO_3$ correspond to transitions into unoccupied O 2*p* states hybridized into the unoccupied Ti 3*d* states [14]. The feature around 532 eV is mainly composed of the t_{2g} subband of the Ti 3*d* states hybridized with O 2*p* state. The intensity below the threshold is expanded by 10 times and is shown with thick line above the XAS spectrum in order to obtain reliable information within the band gap energy region. The arrow shows the top of the valence band. The vertical bar is the position of the Fermi level (E_F), which is determined by the O 1*s* photoemission peak.

One can find that apparent two structures corresponding *a* and *b* peaks are observed in the band gap

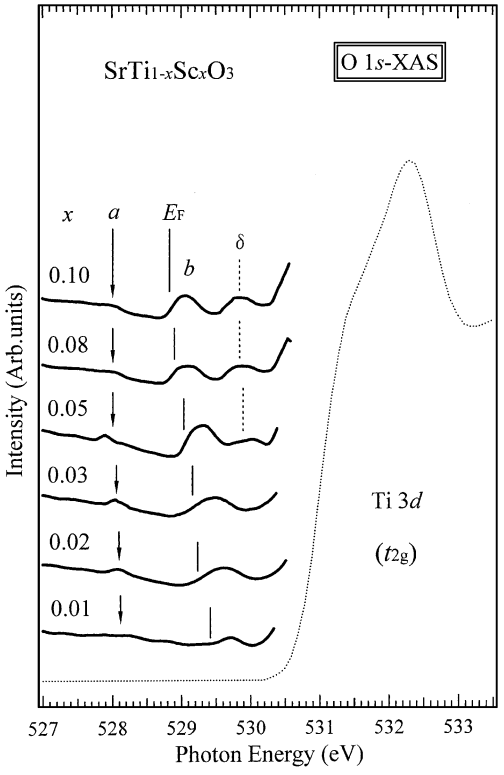

Fig. 1. O 1*s* XAS spectra of dried $SrTi_{1-x}Sc_xO_3$ ($x = 0$–0.10). Thick lines show the O 1*s* XAS spectra in the band gap energy region on an expanded scale. Arrow shows the top of the valence band. Vertical lines show the position of the Fermi level (E_F).

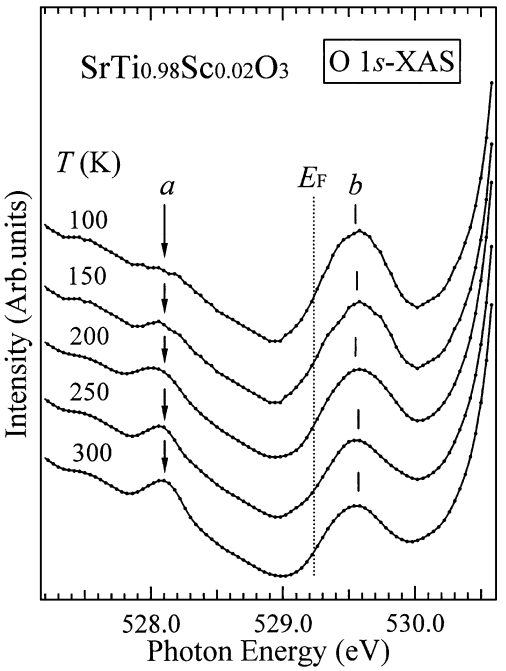

Fig. 2. Temperature dependence of O 1*s* XAS spectra of dried $SrTi_{0.98}Sc_{0.02}O_3$.

energy region of $SrTi_{1-x}Sc_xO_3$. The intensities of *a* and *b* peaks increase with increasing Sc dopant concentration. The *a* peak might be assigned to holes created by Sc doping at the top of the valence band. From the absorption spectra of vacuum ultraviolet region, it has been reported that the band gap of $SrTi_{1-x}Sc_xO_3$ increases with increasing Sc dopant concentration, indicating the formation of holes created at the top of the valence band. The existence of hole in the O 1*s* XAS spectrum is directly evidence of the increasing of the band gap. The *b* peak at near might be assigned to the acceptor-induced level, since it lies just above E_F. On the other hand, δ peak is found at the bottom of the conduction band in the O 1*s* XAS spectra of $x>0.05$. The intensity of δ peak increases with increasing Sc dopant concentration. Such a structure is already reported in the O 1*s* XAS study on $InO_{1.5}$-doped $CaZrO_3$. The δ peak is considered to be a defect-induced level of Ti 3*d* state because the Sc dopant concentration is more than the solubility limit in $SrTiO_3$.

To further clarify the origin of the two structures *a* and *b*, the temperature dependence of O 1*s* XAS spectra has been confirmed in $SrTi_{0.98}Sc_{0.02}O_3$ as shown in Fig. 2. The spectra have been measured in the temperature region from 300 to 80 K. The intensities of XAS spectra are normalized by the peak intensities of Sr 4*d*, though Sr 4*d* line is not shown in this figure. The intensity of *a* peak decreases with decreasing temperature. The intensities of *a* and *b* peaks are plotted in Fig. 3(b), where log (Intensity) is plotted against $1000/T$ (K^{-1}). The *a* and *b* peak intensities are obtained by the subtraction of a linear or a polynominal smooth background. The peak intensity is in arbitrary unit, so that the log (Intensity) scale is not determined by a constant and the slope does not change. The slope of each thick line shown in *a* and *b* peaks is exponential-like, which reflects the activation energy (E_A) from XAS measurement. The estimated value is 0.70 eV for *a* peak and 0.72 eV for *b* peak. The E_A of *a* peak corresponds to that of *b* peak. Furthermore, the value is nearly same value with E_A from the Arrhenius plot of $SrTi_{0.98}Sc_{0.02}O_3$. On one hand, this fact indicates that the electrons of the top of the valence band (*a* peak) are excited thermally to the acceptor-induced level (*b* peak).

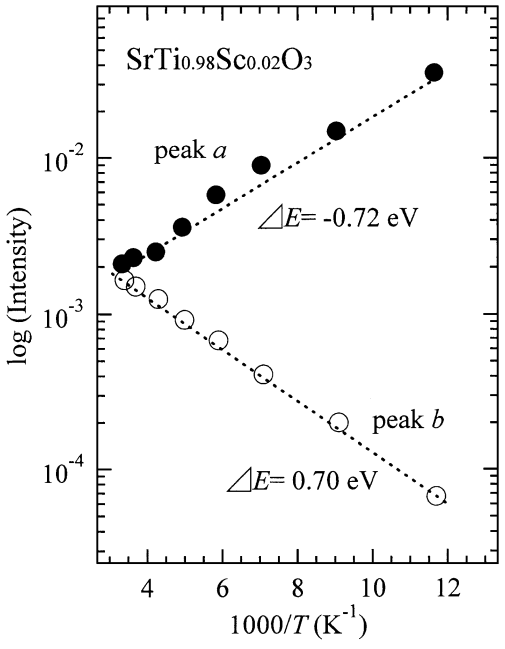

Fig. 3. The plot of intensities of *a* (open circle) and *b* (closed circle) peaks of O 1*s* XAS spectra shown in Fig. 2.

Fig. 4 shows E_A as a function of Sc doping in $SrTi_{1-x}Sc_xO_3$ estimated from the method of Figs. 2 and 3. As a reference, E_A from the slope of the Arrhenius plot is also shown [16,17]. The E_A rapidly decreases to 0.62 eV at $x=0.02$ and slowly increases at $x>0.02$. In $0.01 \le x \le 0.05$, the behavior of E_A from the Arrhenius plot is in good agreement with that of XAS. This fact indicates that the electrical conductivity is attributed between the top of the valence band (*a* peak) and the acceptor-induced level at near E_F (*b* peak). The energy difference of E_A between the Arrhenius plot and the XAS is about ~ 0.1 eV, which contributes the difference between the experimental system. The estimation of the intensity in XAS brings about an error of 0.1 eV so that the total resolution of the experimental system is about 0.1 eV.

In the case of $x>0.05$, however, the behavior of E_A from the Arrhenius plot is not in good agreement with that of XAS. This fact is due to the doping limit of solid solution. The doping limit is $x=0.05$ for $SrTi_{1-x}Sc_xO_3$. In the O 1*s* XAS spectra at $x>0.05$ are found large defect-induced level under the bottom of the Ti 3*d* conduction band, as shown in Fig. 1. The difference of E_A between the Arrhenius plot and XAS is considered to contribute to the mixed conductivity

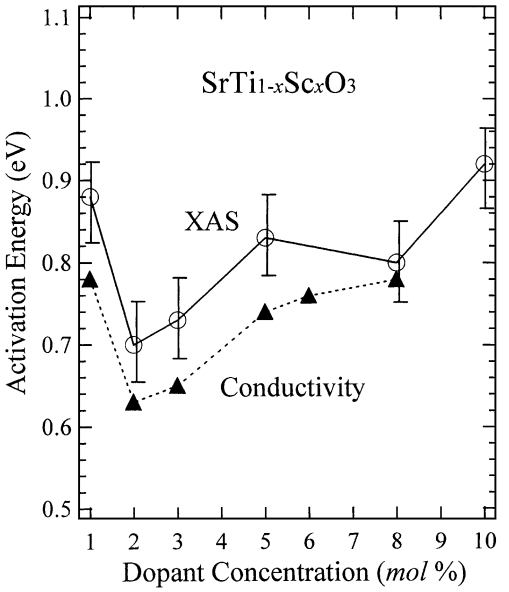

Fig. 4. Activation energy as a function of doping of dried $SrTi_{1-x}Sc_xO_3$ ($x=0-0.10$) estimated from Fig. 2. As a reference, the activation energy from the electrical conductivity is also shown.

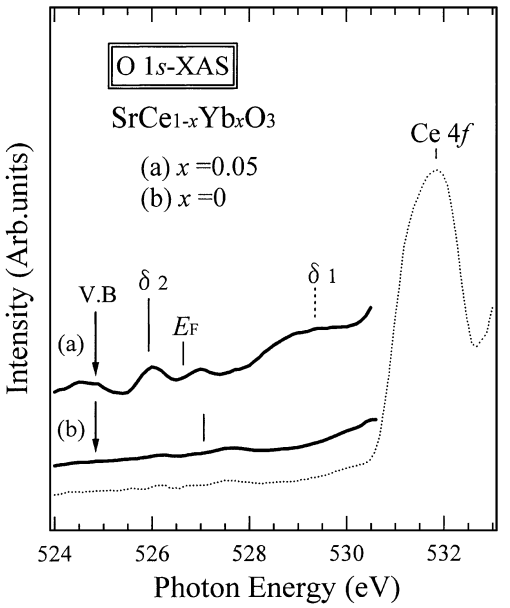

Fig. 5. O 1*s* XAS spectra of $SrCe_{1-x}Yb_xO_3$ ($x=0$, 0.05). Thick lines show the O 1*s* XAS spectra in the band gap energy region on an expanded scale. Arrow shows the top of the valence band. Vertical lines show the position of the Fermi level (E_F).

of both hole and defect that formed above the solubility limit, though the reason has not been clarified thus far.

Fig. 5 shows the O 1*s* XAS spectra of $SrCe_{1-x}Yb_xO_3$. A feature around 532 eV is mainly composed of the unoccupied Ce 4*f* states hybridized with O 2*p* state because the O 1*s* XAS spectra of $SrCeO_3$ correspond to transitions into unoccupied O 2*p* states hybridized into the unoccupied Ce 4*f* states. The intensity below the threshold is expanded 10 times and is shown by the thick line above the XAS spectrum in order to obtain reliable information within the band gap energy region. The arrow is the top of the valence band (V.B). The vertical bar is the position of the Fermi level (E_F).

There is no structure in the band gap of non-doped $SrCeO_3$. However, several features are observed in $SrCe_{0.95}Yb_{0.05}O_3$. A feature near V.B is assigned to holes created by Yb doping at the top of the valence band. This fact has been supported from the absorption spectra of vacuum ultraviolet region [18]. A small feature above E_F is assigned to the acceptor-induced level, since it lies just above E_F. On the other hand, new two features shown by δ_1 and δ_2 are observed in

the band gap energy region, which are not observed in $SrTi_{1-x}Sc_xO_3$ of Fig. 1. The origin of the δ_1 and δ_2 structures is different from $SrTi_{1-x}Sc_xO_3$, since the solubility limit of the dopant concentration is $x<0.10$ in $SrCe_{1-x}Yb_xO_3$. Two structures resembling the above have been also reported in In-doped $CaZrO_3$ [12]. Then, Yamaguchi et al. [12] suggest the presence of defect-induced O 2*p* level, which may be a localized state or an ensemble of defect-induced local band deformed by the presence of an oxygen vacancy, although the evidence has not been shown. Therefore, considering that the protonic conductivity of $SrCeO_3$ is higher than that of $SrTiO_3$, the nature of the defect-induced structure would be one of the most important subjects for the mechanism of protonic conduction.

4. Conclusion

We have studied the electronic structure in the band gap energy region of $SrTi_{1-x}Sc_xO_3$ and $SrCe_{1-x}Yb_xO_3$ using XAS. The O 1*s* XAS spectra of $SrTi_{1-x}Sc_xO_3$ and $SrCe_{1-x}Yb_xO_3$ show two features, which correspond to hole at the top of the valence band and the acceptor-induced level at near E_F. Furthermore, the O 1*s* XAS spectra of $SrCe_{1-x}Yb_xO_3$ show two defect-induced features, which are not observed in those of $SrTi_{1-x}Sc_xO_3$.

Acknowledgements

We would like to thank Dr. T. Yokoya and Dr. A. Chainani for their valuable discussions. We also would like to thank Ms. A. Fukushima for his technical support in performing XAS measurements. This work was partially supported by Foundation for Material Science and Technology of Japan (MST Foundation), the Grant-In-Aid for Science Research (no. 13740191) from the Ministry of Education, Culture and Science of Japan.

References

[1] H. Iwahara, T. Esaka, H. Uchida, N. Maeda, Solid State Ionics 3–4 (1980) 359.
[2] H.H. Huang, M. Ishigame, S. Shin, Solid State Ionics 47 (1991) 251.
[3] S. Shin, H.H. Huang, M. Ishigame, H. Iwahara, Solid State Ionics 40/41 (1990) 910.
[4] N. Sata, K. Hiramoto, M. Ishigame, S. Hosoya, N. Niimura, S. Shin, Phys. Rev., B 54 (1996) 15795.
[5] N. Sata, S. Shin, K. Shibata, M. Ishigame, J. Phys. Soc. Jpn. 68 (1999) 3600.
[6] K. Kurita, N. Fukatsu, T. Ohashi, J. Electrochem. Soc. 142 (1995) 1552.
[7] K. Kobayashi, S. Yamaguchi, Y. Iguchi, Solid State Ionics 108 (1998) 355.
[8] S. Yamaguchi, K. Nakamura, T. Higuchi, S. Shin, Y. Iguchi, Solid State Ionics 136–137 (2000) 191.
[9] T. Higuchi, T. Tsukamoto, N. Sata, M. Ishigame, Y. Tezuka, S. Shin, Phys. Rev., B 57 (1998) 6978.
[10] T. Higuchi, T. Tsukamoto, N. Sata, M. Ishigame, Y. Tezuka, S. Shin, Solid State Ionics 108 (1998) 349.
[11] T. Higuchi, T. Tsukamoto, K. Kobayashi, S. Yamaguchi, Y. Tezuka, S. Shin, Jpn. J. Appl. Phys. 39 (2000) L133.
[12] S. Yamaguchi, K. Kobayashi, T. Higuchi, S. Shin, Y. Iguchi, Solid State Ionics 136–137 (2000) 305–311.
[13] T. Higuchi, T. Tsukamoto, N. Sata, M. Ishigame, K. Kobayashi, S. Yamaguchi, Y. Ishiwata, T. Yokoya, M. Fujisawa, S. Shin, Solid State Ionics 136–137 (2000) 261.
[14] T. Higuchi, T. Tsukamoto, K. Kobayashi, S. Yamaguchi, Y. Ishiwata, T. Yokoya, M. Fujisawa, S. Shin, Phys. Rev., B 61 (2000) 12860.
[15] M. Fujisawa, A. Harasawa, A. Agui, M. Watanabe, A. Kakizaki, S. Shin, T. Ishii, T. Kita, T. Harada, Y. Saitoh, S. Suga, Rev. Sci. Instrum. 67 (1996) 345.
[16] T. Higuchi, T. Tsukamoto, Y. Ishiwata, K. Hiramoto, N. Sata, M. Ishigame, S. Yamaguchi, S. Shin, Phys. Rev., B 65 (2002) 033201.
[17] T. Higuchi, T. Tsukamoto, K. Hiramoto, N. Sata, M. Ishigame, S. Shin, Jpn. J. Appl. Phys. 41 (2002) 2120.
[18] M. Matsumoto, K. Soda, K. Ichikawa, Y. Taguchi, K. Jouda, M. Kageyama, S. Tanaka, N. Sata, Y. Tezuka, S. Shin, S. Kimura, O. Aita, J. Electron Spectrosc. Relat. Phenom. 78 (1996) 179.